

AperTO - Archivio Istituzionale Open Access dell'Università di Torino

Multi-technique study of He⁺ micro-irradiation effects on natural quartz crystals contained in archaeological pottery

This is the author's manuscript

Original Citation:

Availability:

This version is available <http://hdl.handle.net/2318/1742559> since 2020-10-09T22:17:17Z

Published version:

DOI:10.1016/j.nimb.2020.06.035

Terms of use:

Open Access

Anyone can freely access the full text of works made available as "Open Access". Works made available under a Creative Commons license can be used according to the terms and conditions of said license. Use of all other works requires consent of the right holder (author or publisher) if not exempted from copyright protection by the applicable law.

(Article begins on next page)

Multi-technique study of He⁺ micro-irradiation effects on natural quartz crystals contained in archaeological pottery

Laura Guidorzi ^{a,b,*}, Alessandro Re ^{a,b}, Federico Picollo ^{a,b}, Pietro Aprà ^{a,b}, Fulvio Fantino ^c, Luca Martire ^d, Gilberto Artioli ^e, Luca Peruzzo ^f, Sandra Boesso ^e, Valentino Rigato ^g, Leonardo La Torre ^g, Alessandro Lo Giudice ^{a,b}

^a Dipartimento di Fisica, Università degli Studi di Torino, Via Pietro Giuria 1, 10125 Torino (Italy)

^b INFN – Sezione di Torino, Via Pietro Giuria 1, 10125 Torino (Italy)

^c TecnArt S.r.l., Via Modena, 58, 10153 Torino (Italy)

^d Dipartimento di Scienze della Terra, Università degli Studi di Torino, Via Valperga Caluso 35, 10125 Torino (Italy)

^e Dipartimento di Geoscienze, Università degli Studi di Padova, Via Giovanni Gradenigo 6, 35131 Padova (Italy)

^f CNR, Istituto di Geoscienze e Georisorse, via Giovanni Gradenigo 6, 35131 Padova (Italy)

^g INFN - Laboratori Nazionali di Legnaro, Viale dell'Università, 2, 35020 Legnaro, Padova (Italy)

* Corresponding author

Ph: +39 011 670 7365

e-mail: laura.guidorzi@unito.it

Abstract

The effect of α irradiation on natural quartz is commonly known in geology, resulting in the formation of luminescent halos around radioactive inclusions. In archaeological ceramics quartz grains are present and can be surrounded by radioisotopes contained in the clay. The aim of this study is a first attempt to detect similar halos on the outer rims of quartz grains isolated from archaeological pottery. Such identification could be of interest in luminescence dating and as an alternative method for ceramic artworks authentication. Isolated grains were characterized with cathodoluminescence imaging, SEM-EDX and Raman spectroscopy. Some of the crystals were irradiated for reference with a microbeam of He⁺ accelerated ions and investigated by means of real-time ionoluminescence. Obtained results seem to confirm that the natural effect on archaeological quartz might be too weak to be detected with these techniques and underline the importance of the multi-technique approach to avoid misinterpretations.

Keywords: quartz; alpha irradiation; radiation halos; authentication; cathodoluminescence; ionoluminescence

1. Introduction

Quartz is one of the most abundant minerals in the Earth's crust and it has nowadays massive employment for technological applications, such as in semiconductor industry and optoelectronics. For the monitoring and tailoring of specific properties, the structure of SiO₂ has been widely studied in the last few decades, together with the effects of lattice defects and extrinsic impurities [1–5]. These defects affect greatly the luminescent and electronical behavior of SiO₂, both in its crystal and amorphous phase, and can arise, for example, from the damage induced by different types of radiation [6–9].

The effect of α particles on natural quartz is well known in geological studies as the consequence of constant irradiation, for millions of years, of the portion of crystal surrounding radioactive inclusions, in particular U- and Th-bearing phases. α particles are capable of inducing lattice damage, that results in the formation of a visible luminescent halo easily detectable with cathodoluminescence (CL) imaging [10,11]. For a better understanding of this phenomenon, studies by means of He²⁺ or He⁺ artificial implantation at large facilities on both natural and synthetic quartz have been performed and can be found in the literature [12–14]. CL is the most common technique used in this case to detect the halos [10–15], but also Raman spectroscopy [15] and transmission electron microscopy with selected area electron diffraction (TEM-SAED) [13] have been reported. In these works the width of the halo, namely the penetration range of the particles in quartz, varies between 14 and 45 μm depending on the energy of the implanted particle (table 1). Very often, imaging is correlated with an electron paramagnetic resonance (EPR) analysis, aiming to identify the nature of produced

defects: these are generally acknowledged as unpaired electrons at oxygen vacancies (E'_{1} centers) or Non-Bridging Oxygen Hole Centers (NBOHC) [13,16], as well as hole centers due to silicon vacancies [11]. Experiments with the same techniques have also been performed on other types of crystals, for example on zircon [17], albite [18] or $CePO_4$ [19]. It is worth noting that the lattice damage in quartz grains can be partially or totally recovered by means of thermal annealing, at temperatures depending on the type of defects. This effect can be observed, for example, in CL spectra from radiation-damaged halos, where the ultraviolet band is annealed out at 600°C, whereas the red band remains active up to 800°C [16].

Small quartz grains are also usually contained in the clay matrix of ceramic archaeological objects, with a size that varies from some millimeters down to less than 1 micron. These grains are subjected to the same type of α natural irradiation both from the radioactive inclusions of the ceramic mixture and from the environment, especially if the objects remain buried. Moreover, in natural conditions, quartz grains inside archaeological artefacts are also hit by β and γ particles, generated mainly by the decay of ^{40}K , in addition to the decay of isotopes belonging to the Uranium and Thorium chains. All these types of particles induce charges in the material, a condition that is exploited in dating and authentication methods, such as thermoluminescence [20–23], but only α particles cause also a significant damage in the crystal lattice. Since the penetration range of an α particle is smaller than β or γ ones, and emitter isotopes are normally less present inside the grains than outside, only the surface shell of quartz crystals is involved in the interaction with the α irradiation and could show the characteristic traces. Considering that the maximum energy of α particles in natural decays (around 9 MeV) correspond to a maximum penetration depth of about 50 μm (table 1 and SRIM calculation [24]), grains with a diameter larger than 100 μm are needed to be able to detect a clear distinction with the core. It has to be highlighted that the possibility to observe such irradiation profile could be relevant in authentication of ceramics. The more skilled counterfeiters are in fact able to apply an artificial irradiation to a forgery, inducing a false thermoluminescence signal in order to “age” it and cheat the method [25]. However, the artificial irradiation for this purpose can only be done using X-rays or γ -rays, that have a penetration range sufficient to homogeneously irradiate the whole material. This means that quartz grains in artificially irradiated objects should not present the characteristic traces left by α particles. In fact, in most cases during the ceramic production process, the reached temperature is sufficient to anneal the quartz crystals, eliminating previous damage due to irradiation in geological times; at the same time, α fluences accumulated in a recent fake are negligible. To the best of our knowledge, no study has been reported so far on the visible traces that α irradiation can leave on grains of small dimensions in the heterogeneous matrix of archaeological objects. Such radiation-induced halos could also be exploited to define an indirect dating method for ceramics, once a fitting calibration curve is built by correlating α irradiation and halo size. This kind of dating approach has been previously evaluated for geological quartz [10,13,14] without defining a conclusive protocol, due to saturation effects emerging after an irradiation of millions of years or more. This issue is likely to be avoided in the case of archaeological finds, since α fluences accumulated after the thermal annealing are significantly lower, as discussed in section 3.

As first step of this study, that aims at setting the groundwork with the detection and characterization of the halo, quartz crystals enclosed in archaeological material were separated from the clay matrix; then CL images of selected and sectioned grains were acquired for an extensive survey of possible traces. Also, in order to obtain a visual and immediate reference of the effect of α particles on the same natural quartz, some of the embedded grains were irradiated with a microbeam of He^+ accelerated ions at different energies and fluences. Reference irradiated areas have been additionally characterized by means of *in situ* Ionoluminescence, Raman spectroscopy and Scanning Electron Microscope imaging. For the interpretation of results in artificially irradiated sample, it must also be taken into account that α particles lose the greatest part of their energy at the end of their path inside the material, so the highest concentration of generated defects will be at the maximum penetration range (R). This can be calculated by SRIM [24], knowing the density of the material and the energy of the particles.

2. Materials and Methods

Samples were chosen among archaeological building materials, to be able to retrieve a considerable quantity of quartz grains. Moreover, this type of manufactures generally has a coarser ceramic body than artistic pottery, meaning that a higher number of quartz crystals with diameter greater than 100 μm can be extracted. Before the isolation procedure, a measurement of α activity of the whole ceramic powder was made to estimate the total archaeological fluence on the quartz grains. The count rate due to α decays can be easily determined by covering a ZnS scintillator coupled with a photomultiplier with a homogeneous layer of powder (at least 600

mg) [20,26].

The granulometric selection was performed using primarily a 40 μm mesh sieve on the ceramic powder and attempts were made on five archaeological bricks with different grain, color, age and provenance. Only one sample provided an acceptable yield (set at 25% w/w $>40 \mu\text{m}$ minimum) for further treatment of the material: a brick (B1) from the base of Paung Gu Temple in Bagan (Myanmar), dated back to the period between II and late-IV century CE. A chemical processing is generally employed for the isolation of quartz grains with dating purposes [27] and has been also considered for this study as main guideline. A treatment for 1 hour with HCl 10% w/w followed by 1 hour in CH_3COOH 10% w/w allows the elimination of, respectively, carbonates and organic impurities. However, the common use of HF or H_2SiF_6 for the dissolution of feldspars is unsuitable in this case, since these acids also erode, completely or partially, the external shell of the quartz grain, that is the area of interest for this study. After removing traces of phyllosilicates with washings in acetone, partial enrichment in quartz was therefore achieved by magnetic separation using a Frantz L-1 magnetic separator. Further selection was then performed via handpicking of the grains under optical microscope. Finally, the grains were embedded in epoxy resin and polished to expose the core.

The grains were analyzed with a Zeiss EVO 60 Scanning Electron Microscope equipped with a LaB_6 filament and a Bruker Quantax 200 EDX microprobe, setting a working distance of 8.5 mm and a voltage of 20 kV to perform elemental analysis and to confirm the quartz nature of the grains. Measurements were carried out at variable pressure, with 50 Pa in the chamber. The evaluation of shape and dimensions was performed by means of particle analysis on SEM backscattered electrons (BSE) images using Fiji software, an open-source image processing package based on ImageJ. Images with enhanced contrast were converted in binary, then “watershed” feature from BioVoxel toolbox [28] was applied to separate inter-touching particles and it was followed by an extended particle analysis. Three parameters were considered in particular: the Minimum Feret diameter (MinFeret), that is the shortest distance between any two parallels tangent to the grain perimeter; the Aspect Ratio, defined by the ISO 9276-6 guidelines [29] as the ratio of the Minimum Feret diameter to the Maximum Feret diameter, so that the value is always in the range between 0 and 1 (being exactly equal to 1 for the perfectly spherical particle); the Circularity, that also takes in consideration the perimeter (P) and is defined as given in equation 1, where A is the particle area.

$$C = \sqrt{(4\pi A)/P^2} \quad (1)$$

The cold-CL apparatus employed for characterizing the grains is a CITL Cold Cathode Luminescence 8200 mk3 instrument equipped with a polarized optical microscope Olympus BH2 and a Peltier-cooled Olympus DP74 camera. Samples are placed in a vacuum chamber with transparent windows where the pressure is maintained at about 0.8 mbar. An accelerating voltage and current of 15 kV and 500 μA respectively were used during the measurements. The optimal exposition time for CL image acquisition using standard camera conditions was 60 s.

Some of the embedded grains were then carbon-coated and irradiated in vacuum at room temperature. Irradiations have been carried out with a microbeam of He^+ ions at the AN2000 accelerator of the INFN-LNL laboratories in Legnaro (Padova, Italy), dedicated to ion beam-based interdisciplinary research [30–33]. The size of the beam was about 6 μm and an energy of 1.8 MeV for the ions was selected, aiming at best simulating the natural particles. From SRIM simulations, a 1800 keV α particle in quartz (density = 2.65 g/cm^3) can reach a R value of 5.2 μm . To obtain an R compatible with the area of the crystal investigated with a CL probe (R about 2 μm for 15 keV electrons, calculated with CASINO software [34]), a second value of energy of 600 keV was also employed. Three different fluences compatible with geological irradiation (10^{15} ions/ cm^2 , 10^{16} ions/ cm^2 and 10^{17} ions/ cm^2) were tested for each energy value on three $100 \times 100 \mu\text{m}^2$ adjacent areas of the same crystal. Ionoluminescence spectra were simultaneously acquired during irradiations, using the setup described in [35] connected to a QEPro Ocean Optics cooled spectrometer and setting an integration time of 60 s.

Finally, Raman measurements have been performed with a Horiba Jobin Yvon HR800 Raman microspectrometer equipped with a 600 lines mm^{-1} diffraction grating. The optical excitation was provided by a continuous 532 nm laser focused with a $20\times$ air objective; with this configuration, the laser spot reaches about 2 μm in diameter and 6 μm in focal depth.

3. Results and discussion

The count rate measured for α particles decay in the powder extracted from sample B1 was 0.0132 ± 0.0001 Bq on a scintillator surface of 13.85 cm^2 . Taking into account the corrections due to geometrical and electronic

aspects [20], this equals a total α particles activity of about $1.1 \cdot 10^{-3}$ Bq/cm², i.e. about $3.5 \cdot 10^4$ α particles/cm²·year. The α dose absorbed by the archaeological sample since its last firing is calculated as 810 ± 110 μ Gy/year, representing the 17% of the overall annual dose employed for the age calculation. All the corrections for water absorption and α efficiency, as thoroughly described in [20], have been applied to obtain this value. Since the brick dated back to the period between II and late-IV century CE, the expected average irradiation is between about $5 \cdot 10^7$ α particles/cm² and $7 \cdot 10^7$ α particles/cm². Considering for the particles an average energy of 5.5 MeV, these fluence values correspond to an energy density, defined as energy provided by α irradiation in the unit volume, of the order of 10^{-2} J/cm³. When the geological fluences chosen for artificial irradiations are taken in consideration, the energy density results to be higher by 7 to 9 orders of magnitude.

The separation performed on the analyzed material from sample B1 resulted in a granulometric distribution of the grains that ranges between 120 μ m and 2.83 mm: the distribution of MinFerret values can be observed in figure 1, showing an average of 700 μ m. Despite their natural irregularities, the grains have an acceptable roundness in shape, with average values for Aspect Ratio and circularity of 0.68 and 0.71 respectively. The dimensions of the grains are therefore optimal for the observation of potential differences between the outer rim and the core. SEM-EDX analysis on a high statistic of grains confirmed that the separation of quartz achieved with the adopted procedure was successful, despite the presence of few K-feldspar grains. K-feldspars are also easily distinguishable for their bright blue cathodoluminescence [27,36,37], characteristic that can help in discarding them before further analyses.

First observations of the selected grains with exposed core under cold-CL showed the typical violet-brownish color for quartz [38], but no evident halos were detectable on the outer rim. This can have a double meaning: first of all, that the possible halo due to geological exposition is not present, probably for the typology of quartz or for the annealing achieved during the fabrication process. Secondly, that the natural irradiation accumulated from the last heating of the brick, of the order of 10^7 α particles/cm², is not sufficient to induce the defects that cause a halo observable with CL at room temperature. It should also be noted that the spatial distribution of radioisotopes within the ceramic matrix can be heterogeneous, enough that their distance from each quartz crystal may influence the presence and size of the halo. Despite none of the crystals observed under CL in this work showed a clear natural halo on the rims, this topic will have to be further investigated when a comparison with other archaeological samples will be performed.

The CL images acquired after artificial He⁺ irradiation at geological fluences clearly show instead the squared shapes of the targeted areas, with increasing CL intensities as the fluence increases (Figure 2b). Moreover, for 600 keV He⁺ ions with a 10^{17} ions/cm² fluence the irradiation outcome results in a completely different CL color, turning from yellow-green to blue. This color change in respect to lower fluences is probably caused by the more severe defective situation reached. On the other hand, using an energy of 1800 keV this blue color does not emerge because of the depth investigated by the CL probe: the majority of the defects induced by a 600 keV irradiation lays on a more superficial layer than for 1800 keV (see for clarity the SRIM simulations shown in figure 3), so the electrons used in cathodoluminescence, that penetrate only 2 μ m in quartz, cannot reach the maximum R value for 1800 keV ions and generate a signal from a less defective area. The CL intensity variation visible between the inner and the outer part of the squared area is instead due to the gaussian shape of the ion beam used for implantation. Comparing these reference irradiated areas with the external rim of the grains, some similarities in CL colors and intensities can be found (see for example figure 2b) in correspondence of few areas, but the effect is not uniformly distributed along the rims. This might be due to local inclusions of extrinsic activators or to different mineralogical species embedded inside the naturally grown quartz crystal.

Areas with a 10^{17} ions/cm² fluence are also noticeable using a simple optical microscope in transmitted light; the detectability of the areas fades with the decreasing fluence and the irradiations at 10^{15} ions/cm² are completely invisible. In SEM backscattered electrons images all the areas are instead observable (figure 2c). The difference in brightness for the areas irradiated at different fluences is not due in this case to chemical heterogeneity, but most probably to local variations of the structural state of the crystal, induced by the irradiation and related to changes in the electron channeling behavior of the material [39]. However, similar differences cannot be found on the borders of the grain, as in BSE images they appear quite homogeneous with the core.

Ionoluminescence spectra acquired *in situ* during irradiation show some features in the UV and in the NIR regions that remain unchanged for all areas and fluences, such as the two adjacent bands at 355-370 nm and the single peak at 945 nm (figure 4). In the visible region two bands are present, one around 450 nm and one centered at 670 nm. As the fluence increases, the yellow-orange band decreases in intensity: this effect is particularly relevant for irradiations at 600 keV, where at the same time the blue band increases (figures 4 and 5). It is interesting to notice that these emission colors for IL reflect also the visible cathodoluminescence in

figure 2b. The band at 670 nm has been generally associated to NBOHC; for the 450 nm band the assignation of activating defects is instead more controversial and some attributions are: ODC II centers (non-relaxed oxygen vacancies), intrinsic recombination of STEs (self-trapped excitons), STE recombination at E' centers [40]. An EPR analysis might be interesting to discriminate between these possibilities, but it would not be suitable for the final intent of this work since it cannot be selective on the micrometrical outer rim of the grains. In any case, the natural origin of our samples reflects in some differences with the literature reference spectra, showing more irregular shapes and a complex convolution of peaks that may derive from the activation by multiple extrinsic impurities.

Raman spectra were also acquired for each irradiated area and for pristine random points on the same crystal. All spectra showed high peaks at 130 cm^{-1} , 208 cm^{-1} and 468 cm^{-1} , characteristics for quartz, and smaller peaks at 268 cm^{-1} , 356 cm^{-1} , 403 cm^{-1} , 513 cm^{-1} , 809 cm^{-1} , 1084 cm^{-1} and 1161 cm^{-1} (figure 6). With the increase of ion fluence, the 468 cm^{-1} peak, related to A_1 mode optic vibrations, suffers from a small blueshift (figure 7a) ascribable to the induced defects, but the trend of this movement does not seem to correlate linearly with the fluence. The shift suffers the reproducibility of the Raman microscope focus, that affects the depth of field (uncertainty of $\sim 1\text{ }\mu\text{m}$). In fact, from figure 3 it can be seen that if the depth of field varies within the error, the analyzed volume may include or almost entirely exclude the Bragg peak for the damage induced by 1800 keV ions. Analyzing the full width at half maximum (FWHM) of the 468 cm^{-1} peak for every irradiation condition, it was noted that the peak slightly enlarges from pristine to irradiated crystal areas; the differences in FWHM between the three fluences employed are not significantly distinguishable considering the standard deviation (SD) on multiple acquisitions, but a trend correlating the peak width and the induced damage can still be identified. Figure 7b highlights that SD is particularly relevant for irradiations at 600 keV with a 10^{17} ions/ cm^2 fluence. Some of the spectra acquired in this area show additional signals: the ones around 615 cm^{-1} and 660 cm^{-1} are not sharp peaks, but more of a broad and quite low band that is however not part of the background. Moreover, a very broad band arises in the range between 1200 cm^{-1} and 1400 cm^{-1} . It was noticed that these features appeared only if the spectrum was acquired from the right-lower part of the square (figure 6). Actually, from the BSE image in figure 2c a diagonal crack can be clearly seen crossing the area: this might suggest that the crystal grew in this point with different orientations, generating a grain boundary that was partially revealed by polishing. It should be stressed at this point the natural origin of the material under investigation and the fact that it was impossible to notice this kind of characteristics during the irradiation sessions. A Raman spectrum was also acquired in one of the points on the outer rim that showed a similar CL color to the reference areas (point in figure 2b, spectrum in figure 8): the Raman fingerprint assessed that this is actually a different crystal, an orthosilicate (KAlSi_3O_8) embedded inside the quartz grain. The unusual CL color, yellowish-green instead of blue, might be due to an alteration of this K-feldspar [36]. Nevertheless, when looking for visible traces of α particles on the rims, one should keep in mind that similar CL colors may arise from very different sources: this highlights the importance to couple CL analysis with other investigative techniques for the aim of this study.

4. Conclusion

For the first time, to the best of our knowledge, an attempt to observe the α radiation-induced luminescent halo already identified in geological quartz grains was made on archaeological samples. The natural origin of the quartz under study, alongside with the small size of the grains and their heterogeneous environment, resulted in a great characterization challenge. The needed coarseness of the grains limited their provenance to just one of the archaeological samples available. CL imaging and Raman spectroscopy were applied in a similar way to geological studies, but no evident halos were detectable on the outer rim of the grains; this confirmed that a natural irradiation of the order of 10^7 α particles/ cm^2 , accumulated from the last heating of the artefact, is not sufficient to induce defects that cause observable effects by means of these techniques. On the other hand, the absence of the halos is a first evidence of the lack of residual geological damaging effects, that could be attributed to the annealing of the material during the fabrication of the ceramics.

This first approach underlined how important it is to combine different analytical techniques when looking for halos caused by external irradiation, in order to avoid misinterpretation. Moreover, the fact that irradiation effects can be discriminated also by means of SEM backscattered electrons images is relevant, as it adds a widespread and immediate method to possibly identify these traces on other archaeological samples. A comparison of the results here presented with analyses on more quartz grains from samples of different ages (and hence exposed to diverse α fluences) will be of great importance especially for the suggested authentication and dating application. He^+ artificial irradiations performed at a micrometrical scale provided a significantly helpful reference not only for CL imaging, but also for Raman spectroscopy. It will also be useful

to perform in the future additional damaging sessions via α irradiation at different energies and fluences, possibly with a subsequent observation of the grain in cross section.

Acknowledgements

The authors wish to warmly thank CHNet, the INFN network of laboratories working in the Cultural Heritage field, for supporting this research in terms of instrumentation and scientific discussion. Thanks are also due to the Ministry of Religious Affairs and Culture of Myanmar for providing the analyzed sample.

Declarations of interest: none

References

- [1] J.A. Weil, A review of electron spin spectroscopy and its application to the study of paramagnetic defects in crystalline quartz, *Phys. Chem. Miner.* 10 (1984) 149–165. doi:10.1007/BF00311472.
- [2] H.G. Lipson, A. Kahan, Infrared characterization of aluminum and hydrogen defect centers in irradiated quartz, *J. Appl. Phys.* 58 (1985) 963–970. doi:10.1063/1.336174.
- [3] L.E. Halliburton, ESR and optical characterization of point defects in quartz, *Int. J. Radiat. Appl. Instrumentation. Part A.* 40 (1989) 859–863. doi:10.1016/0883-2889(89)90007-5.
- [4] P. Cordier, J.P. Morniroli, D. Cherns, Characterization of crystal defects in quartz by large-angle convergent-beam electron diffraction, *Philos. Mag. A Phys. Condens. Matter, Struct. Defects Mech. Prop.* 72 (1995) 1421–1430. doi:10.1080/01418619508236266.
- [5] S.T. Pantelides, Z.Y. Lu, C. Nicklaw, T. Bakos, S.N. Rashkeev, D.M. Fleetwood, R.D. Schrimpf, The E' center and oxygen vacancies in SiO₂, *J. Non. Cryst. Solids.* 354 (2008) 217–223. doi:10.1016/j.jnoncrysol.2007.08.080.
- [6] F. Preusser, M.L. Chithambo, T. Götte, M. Martini, K. Ramseyer, E.J. Sendezera, G.J. Susino, A.G. Wintle, Quartz as a natural luminescence dosimeter, *Earth-Science Rev.* 97 (2009) 184–214. doi:10.1016/j.earscirev.2009.09.006.
- [7] L. Douillard, F. Jollet, J.P. Duraud, R.A.B. Devine, E. Dooryhee, Radiation damage produced in quartz by energetic ions, *Radiat. Eff. Defects Solids Inc. Plasma Sci. Plasma Technol.* 124 (1992) 351–370. doi:10.1080/10420159208228862.
- [8] A. Alessi, S. Agnello, G. Buscarino, M. Cannas, F.M. Gelardi, A. Sporea, D. Sporea, I. Vâță, Alpha and deuteron irradiation effects on silica nanoparticles, *J. Mater. Sci.* 49 (2014) 6475–6484. doi:10.1007/s10853-014-8381-2.

- [9] B. Wang, Y. Yu, I. Pignatelli, G. Sant, M. Bauchy, Nature of radiation-induced defects in quartz, *J. Chem. Phys.* 143 (2015). doi:10.1063/1.4926527.
- [10] M.R. Owen, Radiation-damage halos in quartz, *Geology*. 16 (1988) 529–532. doi:10.1130/0091-7613(1988)016<0529:RDHIQ>2.3.CO;2.
- [11] D. Cerin, J. Götze, Y. Pan, Radiation-Induced Damage In Quartz At the Arrow Uranium Deposit, Southwestern Athabasca Basin, Saskatchewan, *Can. Mineral.* 55 (2017) 457–472. doi:10.3749/canmin.1700003.
- [12] K. Komuro, Y. Horikawa, S. Toyoda, Development of radiation-damage halos in low-quartz: Cathodoluminescence measurement after He⁺ ion implantation, *Mineral. Petrol.* 76 (2002) 261–266. doi:10.1007/s007100200045.
- [13] R. Krickl, L. Nasdala, J. Götze, D. Grambole, R. Wirth, Alpha-irradiation effects in SiO₂, *Eur. J. Mineral.* 20 (2008) 517–522. doi:10.1127/0935-1221/2008/0020-1842.
- [14] T. Okumura, H. Nishido, S. Toyoda, T. Kaneko, S. Kosugi, Y. Sawada, K. Komuro, Evaluation of radiation-damage halos in quartz by cathodoluminescence as a geochronological tool, *Quat. Geochronol.* 3 (2008) 342–345. doi:10.1016/j.quageo.2008.01.006.
- [15] M. Kayama, H. Nishido, S. Toyoda, K. Komuro, K. Ninagawa, Radiation effects on cathodoluminescence of albite, *Am. Mineral.* 96 (2011) 1238–1247. doi:10.2138/am.2011.3780.
- [16] S. Botis, S.M. Nokhrin, Y. Pan, Y. Xu, T. Bonli, V. Sopuck, Natural radiation-induced damage in quartz. I. Correlations between cathodoluminescence colors and paramagnetic defects, *Can. Mineral.* 43 (2005) 1565–1580. doi:10.2113/gscanmin.43.5.1565.
- [17] Y. Tsuchiya, M. Kayama, H. Nishido, Y. Noumi, Cathodoluminescence of synthetic zircon implanted by He⁺ ion, *Geochronometria*. 44 (2017) 129–135. doi:10.1515/geochr-2015-0054.
- [18] M. Kayama, H. Nishido, S. Toyoda, K. Komuro, K. Ninagawa, Combined cathodoluminescence and micro-Raman study of Helium-Ion-Implanted albite, *Spectrosc. Lett.* 44 (2011) 526–529. doi:10.1080/00387010.2011.610415.
- [19] L. Nasdala, D. Grambole, K. Ruschel, Review of effects of radiation damage on the luminescence emission of minerals, and the example of He-irradiated CePO₄, *Mineral. Petrol.* 107 (2013) 441–454. doi:10.1007/s00710-013-0274-6.
- [20] M.J. Aitken, *Thermoluminescence dating*, Academic Press, London, 1985.
- [21] M.R. Krbetschek, J. Götze, A. Dietrich, T. Trautmann, Spectral information from minerals relevant for luminescence dating, *Radiat. Meas.* 27 (1997) 695–748. doi:10.1016/S1350-4487(97)00223-0.
- [22] E. Tema, F. Fantino, E. Ferrara, S. Allegretti, A. Lo Giudice, A. Re, F. Barello, S. Vella, L. Cirillo, M. Gulmini, Archaeological, archaeomagnetic and thermoluminescence investigation of a baked clay

kiln excavated at chieri, northern italy: Contribution to the rescue of our cultural heritage, *Ann. Geophys.* 57 (2014). doi:10.4401/ag-6611.

- [23] E. Tema, F. Fantino, E. Ferrara, A. Lo Giudice, J. Morales, A. Goguitchaichvili, P. Camps, F. Barello, M. Gulmini, Combined archaeomagnetic and thermoluminescence study of a brick kiln excavated at Fontanetto Po (Vercelli, Northern Italy), *J. Archaeol. Sci.* 40 (2013) 2025–2035. doi:10.1016/j.jas.2012.12.011.
- [24] J.F. Ziegler, M.D. Ziegler, J.P. Biersack, SRIM – The stopping and range of ions in matter, *Nucl. Instruments Methods Phys. Res. Sect. B Beam Interact. with Mater. Atoms.* 268 (2010) 1818–1823. doi:10.1016/j.nimb.2010.02.091.
- [25] D. Stoneham, M. Stoneham, Beating the forger: Authenticating ceramic antiquities, *Contemp. Phys.* 51 (2010) 397–411. doi:10.1080/00107514.2010.495250.
- [26] L. Guidorzi, F. Fantino, E. Durisi, M. Ferrero, A. Re, L. Vigorelli, L. Visca, M. Gulmini, G. Dughera, G. Giraud, D. Angelici, E. Panero, A. Lo Giudice, Thermoluminescence dating laboratory improvements tested on an archaeological rescue site in Trino, Vercelli province, Italy, *Proceedings of IMEKO TC4 International Conference on Metrology for Archaeology and Cultural Heritage, MetroArchaeo 2019* (2019) 199-204. ISBN: 978-929900845-4
- [27] P. Guibert, I.K. Bailiff, S. Blain, A.M. Gueli, M. Martini, E. Sibilina, G. Stella, S.O. Troja, Luminescence dating of architectural ceramics from an early medieval abbey: The St Philbert Intercomparison (Loire Atlantique, France), *Radiat. Meas.* 44 (2009) 488–493. doi:10.1016/j.radmeas.2009.06.006.
- [28] J. Brocher, *The BioVoxel Image Processing and Analysis Toolbox*, (2015).
- [29] ISO, Representation of results of particle size analysis – Part 6: Descriptive and quantitative representation of particle shape and morphology, in: *ISO 9276-6:2008(E)*, 2008.
- [30] J. Forneris, A. Lo Giudice, P. Olivero, F. Picollo, A. Re, M. Marinelli, F. Pompili, C. Verona, G.V. Rinati, M. Benetti, D. Cannata, F. Di Pietrantonio, A 3-dimensional interdigitated electrode geometry for the enhancement of charge collection efficiency in diamond detectors, *Europhys. Lett.* 108 (2014). doi:10.1209/0295-5075/108/18001.
- [31] A. Lo Giudice, D. Angelici, A. Re, G. Gariani, A. Borghi, S. Calusi, L. Giuntini, M. Massi, L. Castelli, F. Taccetti, T. Calligaro, C. Pacheco, Q. Lemasson, L. Pichon, B. Moignard, G. Pratesi, M.C. Guidotti, Protocol for lapis lazuli provenance determination: evidence for an Afghan origin of the stones used for ancient carved artefacts kept at the Egyptian Museum of Florence (Italy), *Archaeol. Anthropol. Sci.* 9 (2017) 637–651. doi:10.1007/s12520-016-0430-0.
- [32] A. Battiato, M. Lorusso, E. Bernardi, F. Picollo, F. Bosia, D. Ugues, A. Zelferino, A. Damin, J. Baima, N.M. Pugno, E.P. Ambrosio, P. Olivero, Softening the ultra-stiff: Controlled variation of

Young's modulus in single-crystal diamond by ion implantation, *Acta Mater.* 116 (2016) 95–103.
doi:10.1016/j.actamat.2016.06.019.

- [33] F. Picollo, A. Battiato, E. Bernardi, M. Plaitano, C. Franchino, S. Gosso, A. Pasquarelli, E. Carbone, P. Olivero, V. Carabelli, All-carbon multi-electrode array for real-time in vitro measurements of oxidizable neurotransmitters, *Sci. Rep.* 6 (2016) 1–8. doi:10.1038/srep20682.
- [34] D. Drouin, A.R. Couture, D. Joly, X. Tastet, V. Aimez, R. Gauvin, CASINO V2.42—A Fast and Easy-to-use Modeling Tool for Scanning Electron Microscopy and Microanalysis Users, *Scanning.* 29 (2007) 92–101. doi:10.1002/sca.20000.
- [35] A. Re, D. Angelici, A. Lo Giudice, J. Corsi, S. Allegretti, A.F. Biondi, G. Gariani, S. Calusi, N. Gelli, L. Giuntini, M. Massi, F. Taccetti, L. La Torre, V. Rigato, G. Pratesi, Ion Beam Analysis for the provenance attribution of lapis lazuli used in glyptic art: The case of the “collezione Medicea,” *Nucl. Instruments Methods Phys. Res. Sect. B Beam Interact. with Mater. Atoms.* 348 (2015) 278–284. doi:10.1016/j.nimb.2014.11.060.
- [36] R. Fonseca, H. Couto, IOP Conference Series: Earth and Environmental Science Application of Cathodoluminescence to The Study of Feldspars: Imaging and Spectrometry Related content The temperature dependence of luminescence in some feldspars (80–300 K) S M Barnett and I K Baili, *IOP Conf. Ser. Earth Environ. Sci.* 95 (2017). doi:10.1088/1755-1315/95/3/032029.
- [37] I. Parsons, D.A. Steele, M.R. Lee, C.W. Magee, Titanium as a cathodoluminescence activator in alkali feldspars, *Am. Mineral.* 93 (2008) 875–879. doi:10.2138/am.2008.2711.
- [38] J. Götze, M. Plötze, D. Habermann, Origin, spectral characteristics and practical applications of the cathodoluminescence (CL) of quartz - A review, *Mineral. Petrol.* 71 (2001) 225–250. doi:10.1007/s007100170040.
- [39] L. Nasdala, A. Kronz, J.M. Hanchar, M. Tichomirowa, D.W. Davis, W. Hofmeister, Effects of natural radiation damage on back-scattered electron images of single crystals of minerals, *Am. Mineral.* 91 (2006) 1739–1746. doi:10.2138/am.2006.2241.
- [40] M.L. Crespillo, J.T. Graham, Y. Zhang, W.J. Weber, In-situ luminescence monitoring of ion-induced damage evolution in SiO₂ and Al₂O₃, *J. Lumin.* 172 (2016) 208–218. doi:10.1016/j.jlumin.2015.12.016.

Tables and Images

Ion	Ions energy (MeV)	Fluence (ions/cm ²)	Quartz type (N/S)	Halo width (μm)	Reference
He ⁺	4	10 ¹⁵	S	14	[12]
He ²⁺	8.8	10 ¹³ – 10 ¹⁷	N & S	45	[13]
He ⁺	4	10 ¹⁴ – 10 ¹⁵	N	14	[14]

Table 1. Parameters of previous experiments from the literature with resulting radiation halo width. N = natural, S = synthetic.

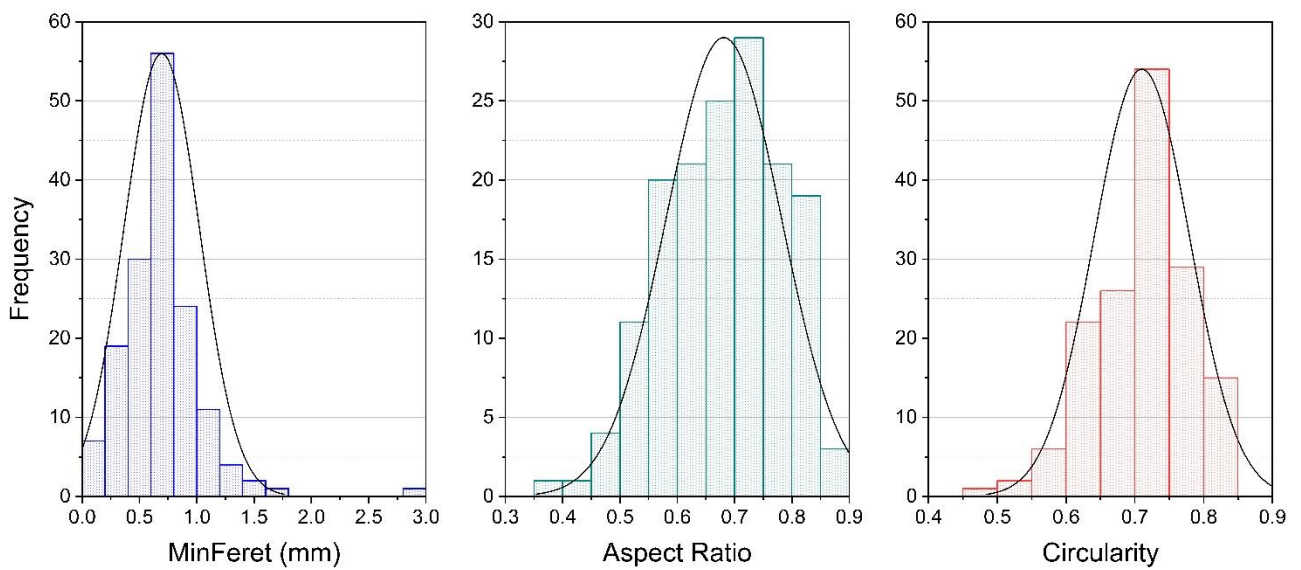


Figure 1. Distributions of Minimum Feret, Aspect Ratio and Circularity for the isolated quartz grains.

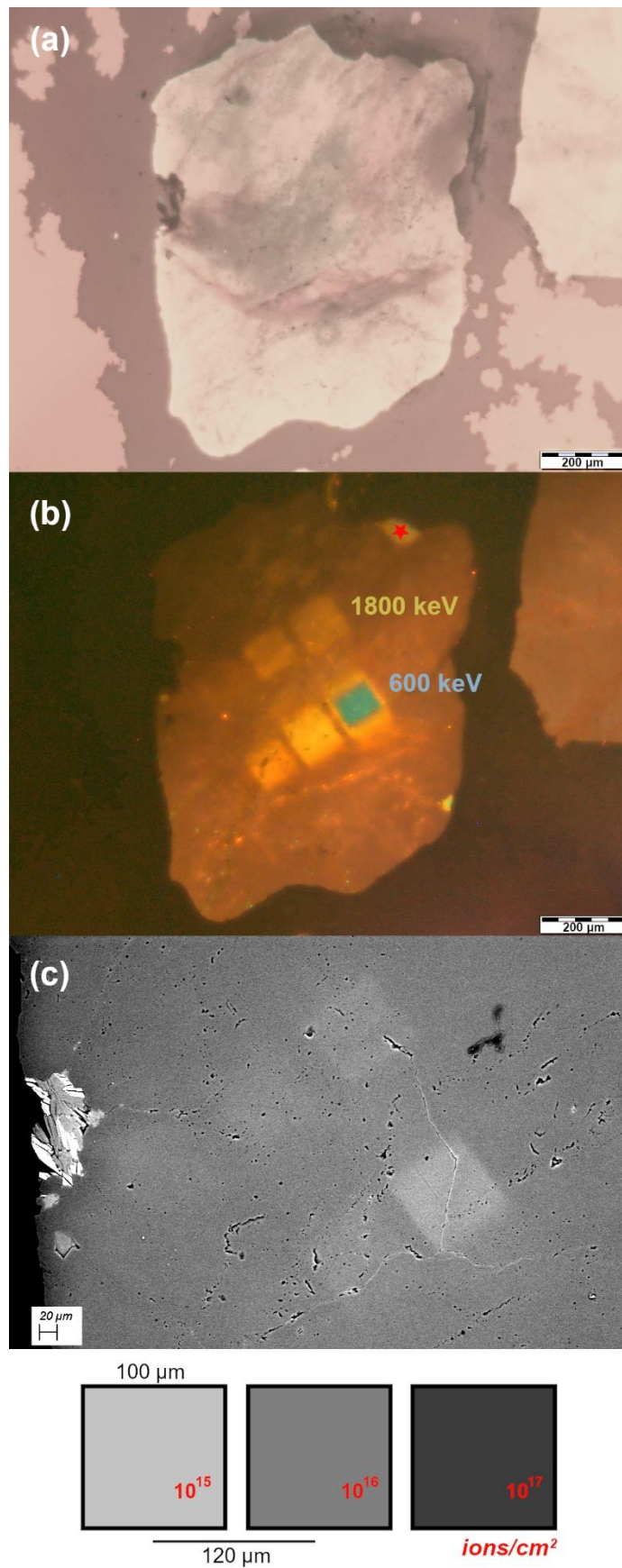


Figure 2. An irradiated quartz grain under (a) optical microscope, (b) cathodoluminescence, (c) SEM-BSE. A scheme of the irradiation pattern is also reported. The red star indicates the point investigated with Raman spectroscopy.

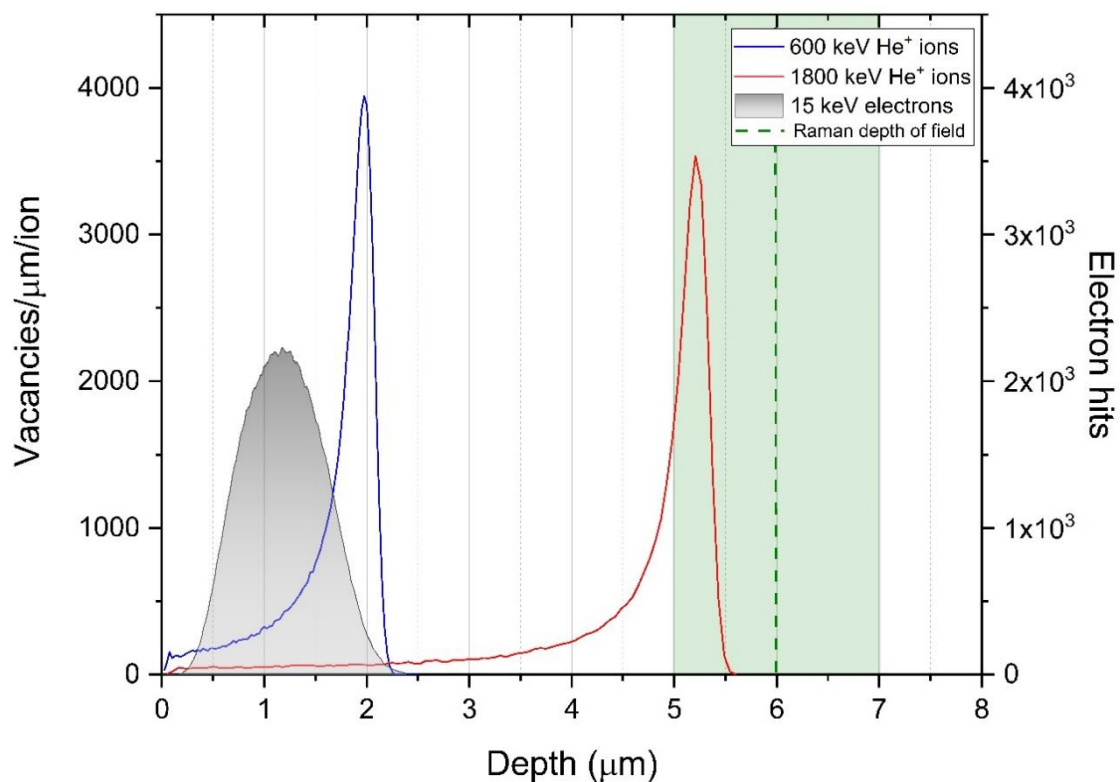


Figure 3. Comparison of depth penetration in quartz between SRIM and CASINO simulations for, respectively, He⁺ damage distributions and 15 keV electron hits distribution. Raman depth of field is also indicated, with an error of $\pm 1 \mu\text{m}$ (green area).

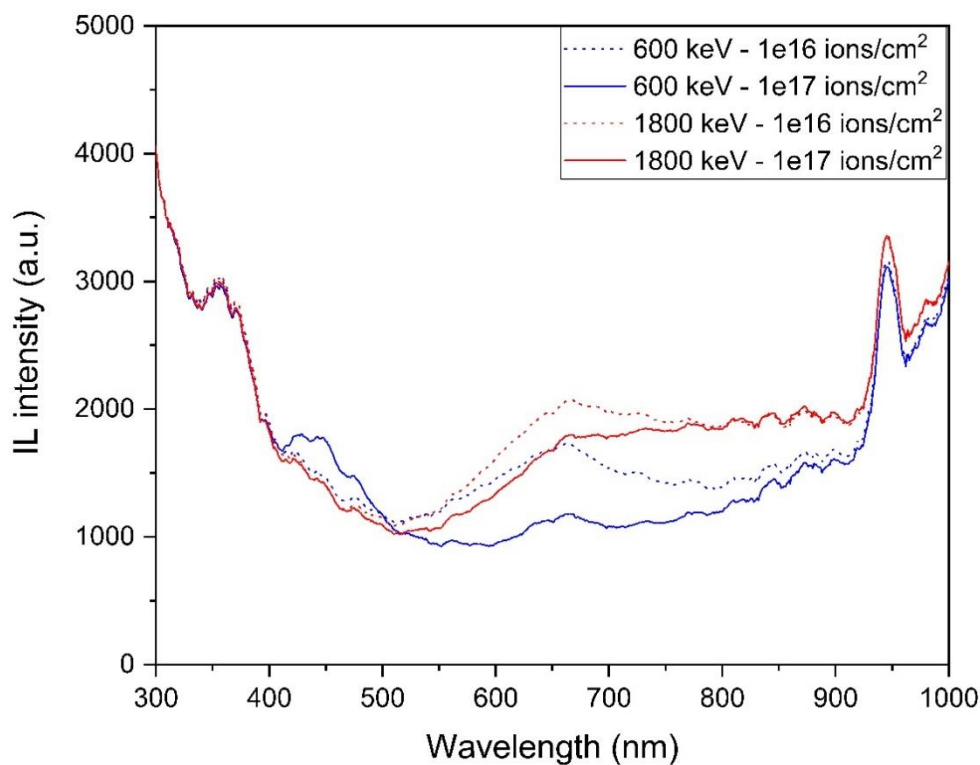


Figure 4. Ionoluminescence spectra showing features in UV, visible and NIR regions. The effect of increasing fluence is appreciable comparing dotted and continuous lines.

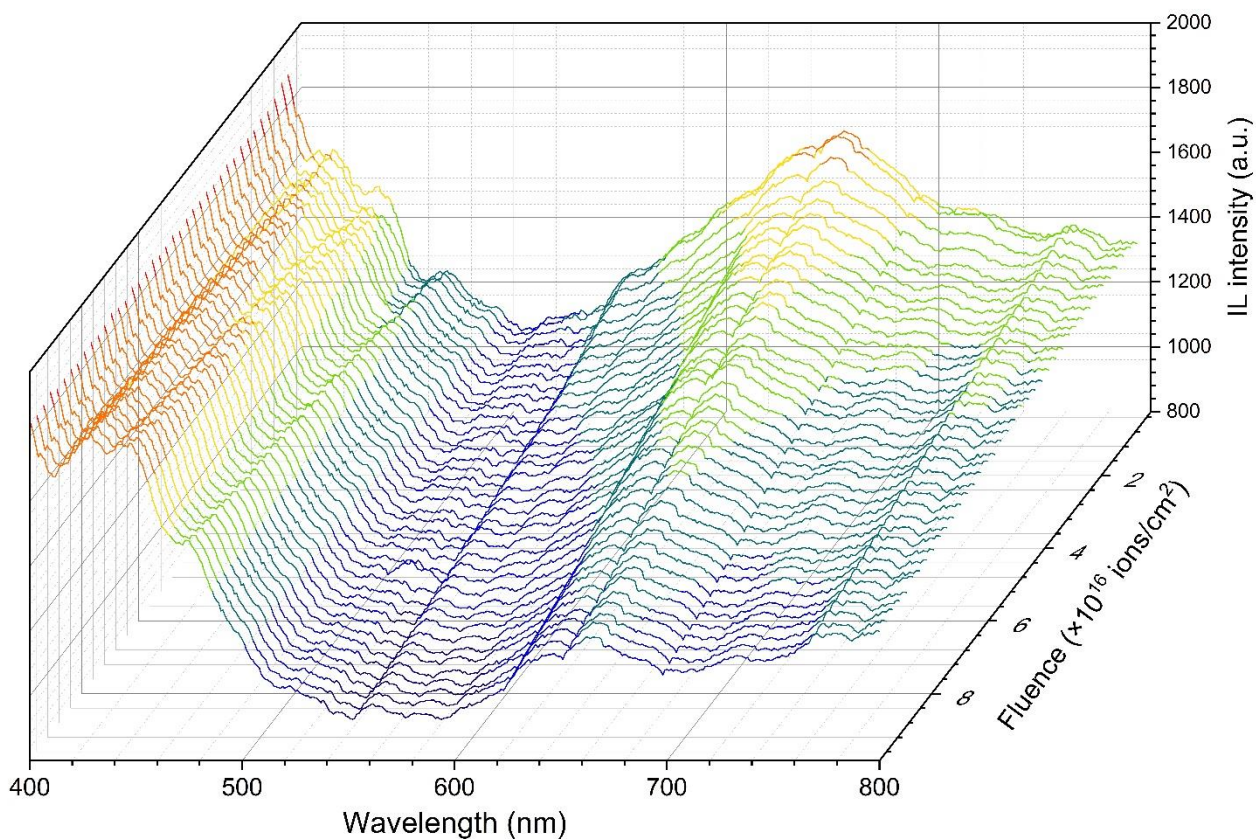


Figure 5. Evolution of *in situ* visible ionoluminescence acquired for irradiations at 600 keV up to 10^{17} ions/cm². This representation clearly shows how, with the constant increment of fluence, the 670 nm band decreases, whereas the 450 nm band slightly increases.

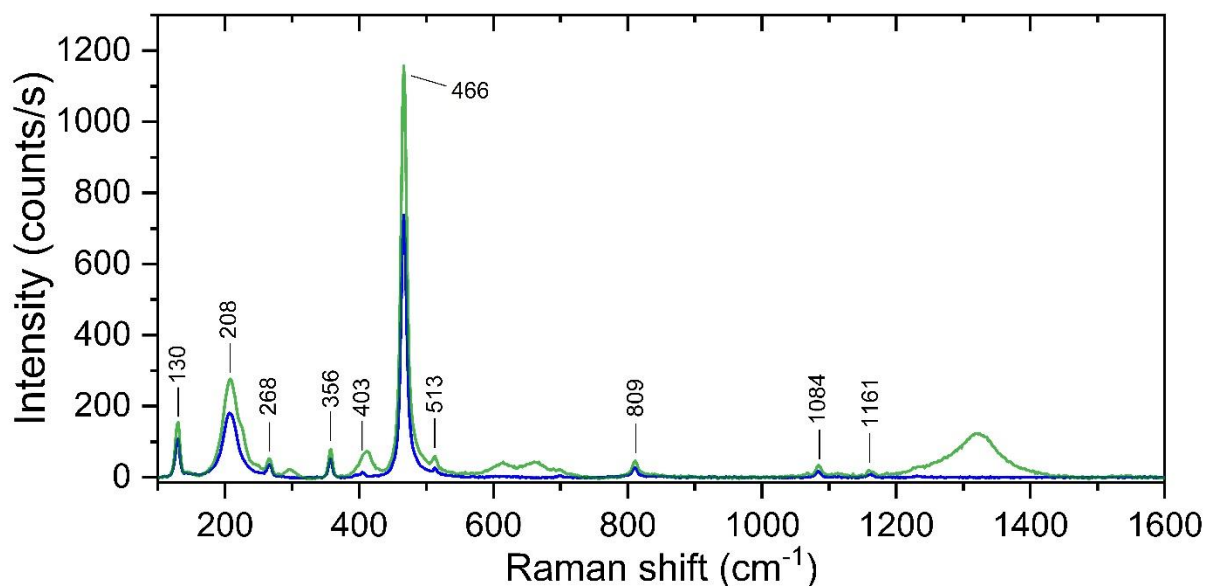


Figure 6. Raman spectra for the area 600 keV- 10^{17} ions/cm². In blue, a spectrum acquired in the left-upper corner of the squared area that exhibits the same peaks as pristine quartz and other irradiated areas; in green, the spectrum from the right-lower corner, showing the additional bands around 290 cm⁻¹, 410 cm⁻¹, 615-660 cm⁻¹ and 1200-1400 cm⁻¹.

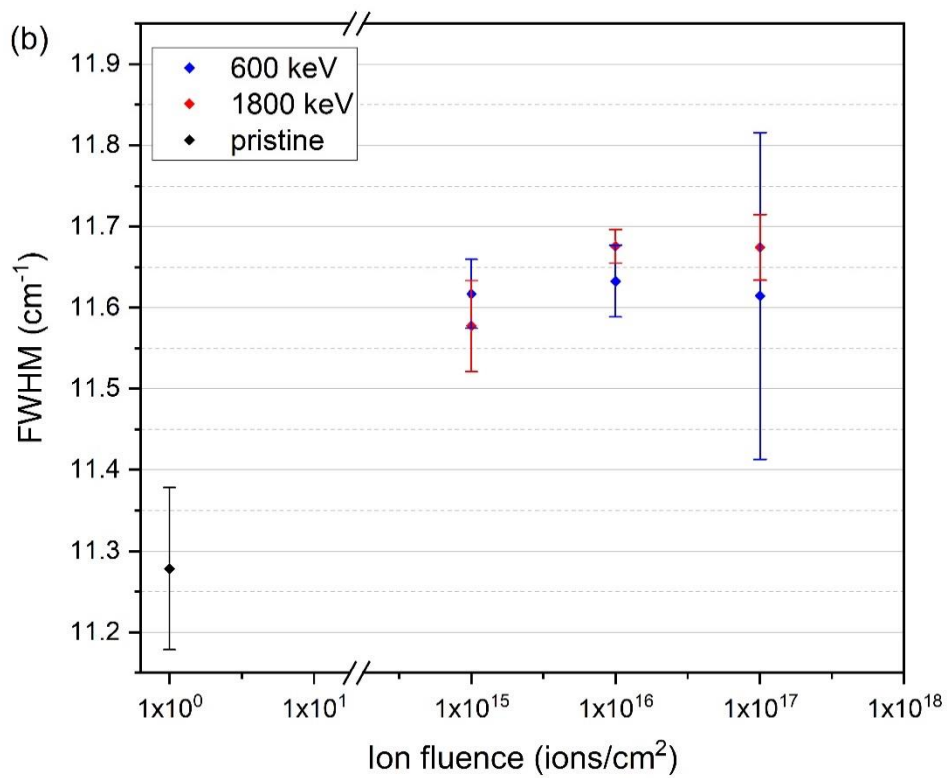
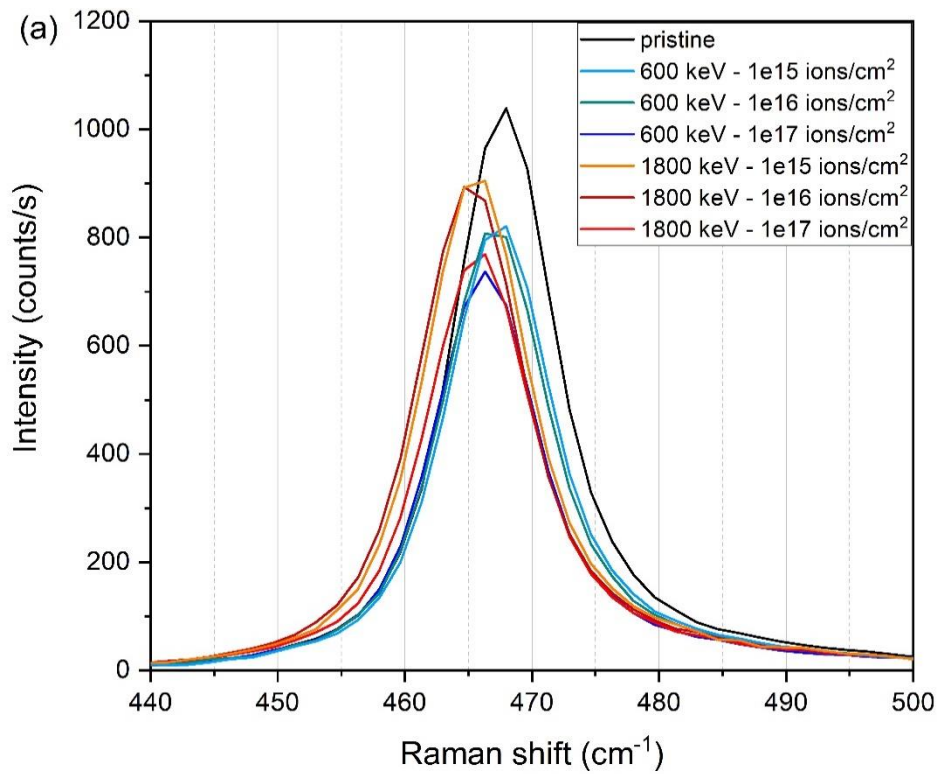


Figure 7. (a) The 468 cm⁻¹ Raman peak of quartz measured for pristine crystal and all irradiation conditions; (b) values of full width at half maximum for the 468 cm⁻¹ Raman peak versus the ion fluence. Error bars represent the standard deviation on at least 4 spectra.

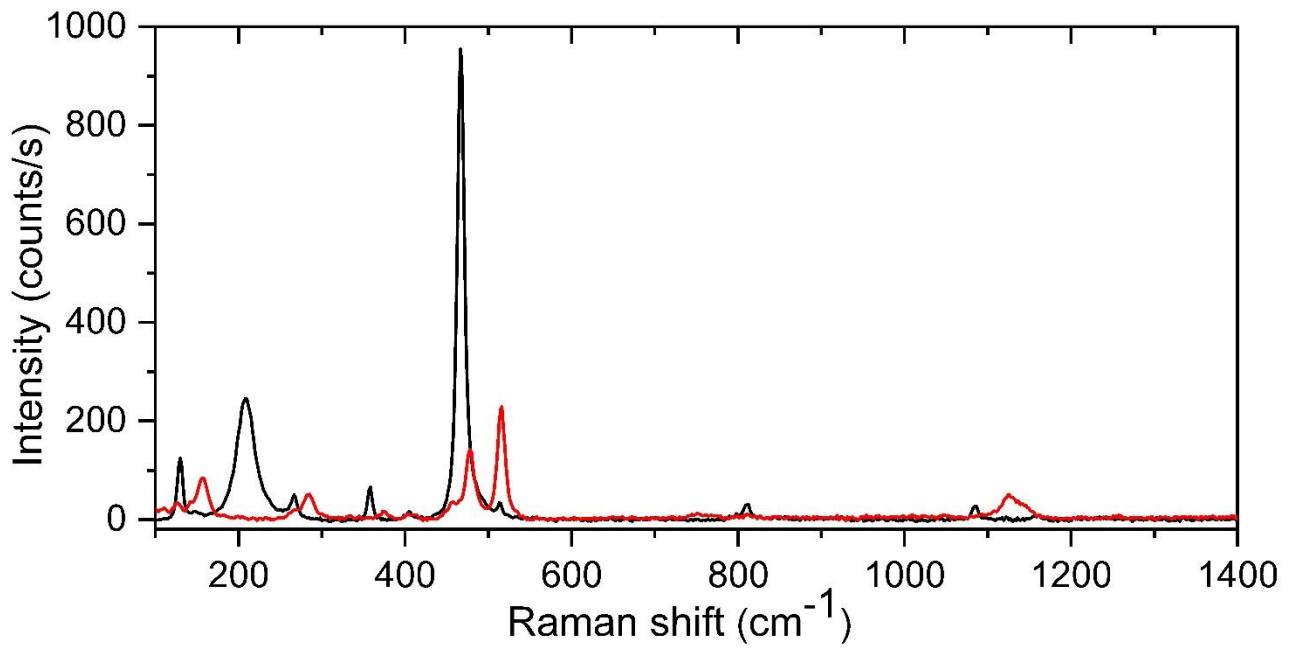


Figure 8. Raman spectra of pristine quartz (black) and of the luminescent area indicated with the red star in figure 2b and identified as an orthoclase inclusion (red).